# Experimental investigation of multi-step stress-relaxation-ageing of 7050 aluminium alloy for different pre-strained conditions

Jing-Hua Zheng, Ran Pan, Chen Li, Wei Zhang, Jianguo Lin, Catrin M. Davies

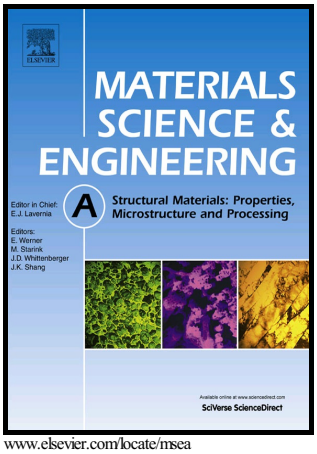


www.elsevier.com/locate/msea

PII: S0921-5093(17)31392-8
DOI: https://doi.org/10.1016/j.msea.2017.10.066
Reference: MSA35669

To appear in: *Materials Science & Engineering A*

Received date: 14 April 2017
Revised date: 20 September 2017
Accepted date: 20 October 2017

Cite this article as: Jing-Hua Zheng, Ran Pan, Chen Li, Wei Zhang, Jianguo Lin and Catrin M. Davies, Experimental investigation of multi-step stress-relaxation-ageing of 7050 aluminium alloy for different pre-strained conditions, *Materials Science & Engineering A,* https://doi.org/10.1016/j.msea.2017.10.066

# Experimental investigation of multi-step stress-relaxation-ageing of 7050 aluminium alloy for different pre-strained conditions

Jing-Hua Zheng[a], Ran Pan[a], Chen. Li[b], Wei Zhang[b], Jianguo Lin[a], Catrin M. Davies [a]*

[a] Department of Mechanical Engineering, Imperial College London, London SW7 2AZ, UK

[b] The First Aircraft Institute, Xi'an, P. R. China

**Abstract**

A novel insight into the whole two-step stress relaxation ageing process during T74 multi–step ageing treatment (120 °C for 6 hours and subsequently 177 °C for 7 hours), which is typically experienced by extra-large aircraft components that contain high residual stresses, has been established. Stress relaxation ageing (SRA) tests, tensile tests and transmission electron microscopy (TEM) were performed on AA7050 samples to determine the relationship between internal microstructure and macroscopic behaviour during the stress relaxation and precipitate evolution process. Samples were subjected to SRA at different initial stresses (220-360 MPa) after being pre-strained to different extents (i.e. 0%, 1%, 3%). Room temperature tensile tests were then performed on interrupted SRA test specimens to examine the corresponding strengthening phenomenon. TEM was performed on a selection of peak–aged and T74 over–aged samples to study the precipitate distribution. At 120 °C typical stress relaxation behaviour was observed and the data followed a logarithmic curve. Subsequently at 177 °C, dislocation–creep dominated stress relaxation behaviour, with no apparent threshold stress, was observed. The absence of a threshold stress at 177 °C may be attributed to the continuous over-ageing phenomenon. The effect of pre-deformation levels and initial stresses on SRA has also been investigated. Pre-stretching, which creates uniformly distributed dislocations, promotes stress relaxation and ageing. No significant influence of initial stress level on SRA was observed at 120 °C, but noticeable effects were seen at 177 °C. The calculated stress exponent *n* at 177 °C is found independent of the initial stresses. These findings provide clear scientific guidance for residual stress reduction during the multi-step ageing process of AA7050 and provide the basis for residual stress prediction models.

**Keywords:** Stress relaxation ageing, residual stress, aluminium alloys, pre-strain, T74 multi–step ageing, precipitation process

## 1 Introduction

Precipitation hardening 7000 series aluminium alloys are widely used for extra-large aircraft structural components. This is due to their excellent mechanical properties, particularly their good strength-to-weight

ratio [1]. In order to meet the strength requirements, a defined sequence of heat treatments and manufacturing processes are employed to ensure the required mechanical properties, microstructures and dimensional accuracy of manufactured components [2]. The typical manufacturing and heat treatment processes for producing extra-large AA7xxx components include:

(i) Multistage hot forging to enable the component's features to be manufactured;

(ii) Solution heat treatment (SHT) followed by quenching to form super-saturate solid solution (SSSS). Quenching can create a significant level of residual stresses into the extra-large aluminium components;

(iii) Multistage cold working (i.e. cold forging) to reduce the level of residual stresses. Due to the large size and complicated features of the forged component, it is very difficult to fully eliminate the residual stresses [3];

(iv) Multistage ageing to get precipitation hardening and required mechanical properties. In this stage, the residual stress will be reduced further;

(v) Machine finishing to achieve required dimensional accuracy;

During machine finishing of the extra-large structural components, more than ~70% of the material is usually removed to achieve the required shape. The residual stresses acting on the cut surface are relieved, resulting in the remaining material deforming to achieve a new interior force equilibrium. This redistribution of the residual stress causes distortion of the machined parts [4]. Thus the dimensional accuracy cannot be guaranteed for the manufactured extra-large aluminium components. The final stage of components' residual stress reduction is the ageing process (iv), which creates the required precipitation hardening and mechanical properties and also thermally activated creep and stress relaxation occurs. Ageing is the final opportunity to get required mechanical properties and reducing residual stresses from the parts so that the quality of the manufactured components can be guaranteed. Significant research has been carried out to study precipitate nucleation and growth during steady state ageing conditions [5-8]. However, limited studies have been performed on residual stress reduction and its effects on the precipitation process during the multistage ageing, which is extremely important for controlling the component's properties. Therefore, a detailed examination of the residual stress reduction, an improved understanding of its effects on the precipitation characteristic is a vital requirement for helping improve the properties and the precision of the manufactured parts.

For AA7xxx, a T74 over-aged temper is normally used to improve the fracture toughness and corrosion resistance by sacrificing 10-15% of the strength. The traditional precipitate evolution process under T74 multi–step temperature exposure, both with and without stress effects, has been widely referenced in literature [9-12]. During the T74 pure ageing treatment, Guinier-Preston (GP) zones are formed rapidly and uniformly at the first low-temperature step, and these GP zones can serve as nuclei at the second high-temperature step, leading to a fast formation of finely dispersed $\eta'$ and $\eta$. Sha et al. [9] and Stiller et al. [11] investigated the precipitation of an Al-Zn-Mg after a multi-step ageing treatment and concluded that two parallel precipitation

routes exist — one involving a formation and dissolution of GP I and the other involving the nucleation of clusters, which is the precursor of $\eta'$. In addition, pre-stretch effects on ageing kinetics have been studied to simulate cold work effects on the precipitation process. It has been proven by many including Waterloo et al. [13], Deschamps et al. [7] and Han et al. [14], that the pre-strain induced dislocations lead to a promotion of ageing, thus a decrease in the alloy's strength and an increase in alloy's fracture toughness after the T74 treatment. Stressed ageing and creep age forming have also been studied. Two peaks in hardness were found by Guo et al. [12, 15] when an alloy experienced an elastic stress smaller than 0.6 of the yield strength during ageing. Chen et al. [16, 17] continues to study creep age forming and simulated age forming behaviour and has suggested that the stress applied leads to finer bulk precipitate distributions, larger precipitate free zones (PFZ), larger discontinuous grain boundary precipitates and elongated grains with higher aspect ratios due to the interaction between creep and precipitation.

Limited research has been performed on the stress relaxation behaviour during ageing. Solberg [18] reported that the stress relaxation behaviour of aluminium alloys at the ageing temperature can be described by the results of the load controlled creep tests under the same conditions, however, the interaction between relaxation and ageing was not discussed in detail. Zhan [1] built a set of creep-ageing constitutive equations to predict the spring back of the components. Spence et. al. [19] predicted surface residual stress reduction at different temperatures using data from constant load creep tests at the respective temperatures. However, data generated from constant load creep tests have not always successfully described stress relaxation ageing behaviour i.e. during strain controlled creep tests [20]. Chen, et al. [17] reported the stress relaxation behaviour during ageing. However, the tests were conducted at constant temperatures. Therefore, to-date, research has not focussed on the stress relaxation ageing behaviour of 7xxx series alloys under multi-step dynamic ageing conditions.

In the aerospace industry, cold stretch or compression is employed before ageing to release the majority of the residual stresses inside the extra-large aluminium component, i.e. stage (iii). The cold work prior to ageing can introduce a certain amount of dislocations and impact the subsequent stress relaxation ageing behaviour. Li et al. [21] reviewed the effect of prior inelastic deformation on creep behaviour of engineering alloys and summarised that both resistance and enhancement effects can be introduced on the subsequent creep response of metallic materials. The pre-tension generally leads to an increase in the creep resistance for stainless steels while a decrease in that for 2.25Cr-1Mo ferritic steel. Regensburger [22] examined aluminium alloy 6016 and obtained an increased creep strain rate by a factor of $(1 + C\varphi^k)$, where $\varphi$ described the equivalent plastic strains, $C$ and $k$ are material constants. Although pre-strain effects have been widely studied, the influence of pre-strains were found to vary between different stress ranges for different alloys, as the microstructure of the alloys vary remarkably due to the increased dislocations in different conditions (e.g. stress range, temperature range, etc). Therefore, it is essential to investigate the room temperature pre-strain effects on 7050 aluminium alloy under its T74 SRA condition.

In this work, the stress relaxation ageing (SRA) behaviour of AA7050 during a T74 multi-step dynamic ageing treatment was investigated. In addition, the prior cold work effects on the subsequent stress relaxation ageing behaviour were also examined. Based on previous findings, as discussed above, this is the first time to the author's knowledge that this work has been performed. Various initial stress conditions were applied to AA7050, which was initially deformed at the room temperature with a total strain of 0%, 1%, 3%, to determine the effects of both the initial stresses and the pre-existing plastic deformation on high temperature relaxation characteristics. Subsequently, the evolution of the yield strength was analysed, through performing room temperature tensile tests on interrupted SRA test samples, to understand the interaction between age hardening and stress relaxation behaviour. Transmission electron microscope (TEM) tests were conducted on a select number of samples to examine the corresponding microstructure evolution during SRA.

## 2 Experimental Programme

### 2.1 Material and specimen design

The material used in this study is a 7050 Al-Zn-Mg-Cu alloy with the chemical composition shown in Table 1. Cylindrical specimens of gauge length of 14 mm were machined from a rolled block such that their principal axes were aligned in the rolling direction. The detailed dimensions are illustrated in Fig. 1 (a). A schematic of stress-relaxation-ageing (SRA) test set up is shown in Fig. 1(b). During the stress relaxation ageing tests, the test specimens were heated in a furnace and the temperature was strictly controlled to be within ± 1 °C of the set temperature by a thermocouple on the sample. An extensometer was attached to the specimen's gauge length to control the sample's strain.

Table 1 Main chemical composition of aluminium alloy 7050, wt%

| Zn | Mg | Cu | Al |
|---|---|---|---|
| 5.7-6.7 | 1.9-2.6 | 2-2.6 | balance |

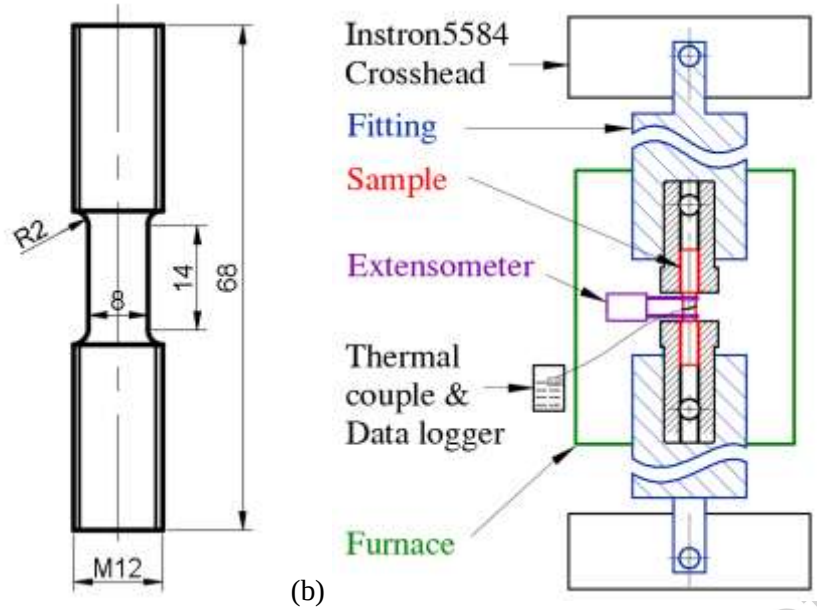


(a) (b)

Fig. 1. (a) SRA specimen geometry (dimensions are in mm) (b) schematic illustration of the SRA test setup

### 2.2 Experimental test procedure

Tests were designed to investigate both the stress relaxation and ageing behaviour of 7050 alloy during a multi-step heat treatment (120 °C × 6 h + 177 °C × 7 h), which is strictly in accordance with the T74 ageing treatment profile for 7050 alloys. The sample preparation and testing procedure are illustrated schematically in Fig. 2. In preparation for the SRA tests, all specimens were firstly solution heat treated at 475 °C for 30 min followed by a quench in warm water (i.e. 60 °C). Subsequently, within an hour after quenching, a selection of samples were pre-strained to a total strain of 1% and 3% with a rate of 0.3% $min^{-1}$. During this time natural ageing will occur hence, for consistency, the samples with no pre-strain were also held at room temperature for an hour. The samples were then stored in a freezer at -20 °C to avoid any further natural ageing.

The SRA test procedure consists of three stages as illustrated in Fig. 2 and described below:

- Stage I: The specimens were loaded in tension to various initial stress levels, $\sigma_i$ (220-360 MPa), with a loading speed of 150 MPa/min, after the temperature had stabilised to 120 °C. The sample was then held in strain control, and hence stress relaxation occurred. The stress was recorded with a 10 s interval. Instead of fixing the movement of the machine's crosshead, which can induce errors due to the complex machine-specimen interactions and leading to un-trustable relaxation results according to [23]. The sample's strain was kept constant using the extensometer attached to the gauge length
- Stage II: The temperature was increased from 120 °C to 177 °C within a period of 1 h. Due to the temperature increase, thermal expansion of the sample and grips caused issues with extensometer strain control. Therefore, the sample was held in stress control at its relaxed stress level during this heat up period.

- Stage III: Samples were held at 177 °C for 7 h, during which the samples were again held in strain control and stress relaxation was monitored.

After the 14 hrs' SRA process, the specimens were air cooled to room temperature. Subsequently, room temperature tensile tests were conducted to determine the mechanical properties of the T74 SRA samples.

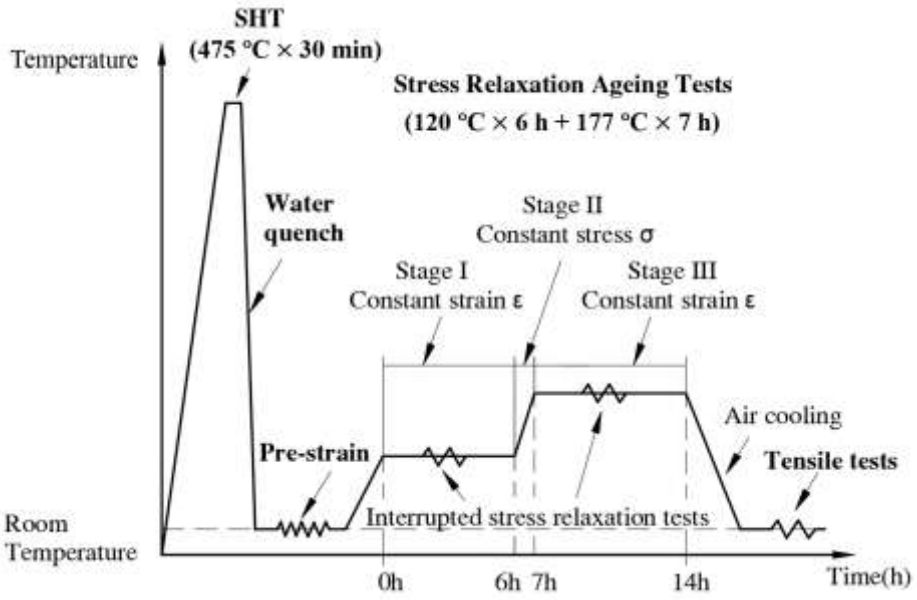


Fig. 2. Schematic illustration of the sample preparation and SRA procedure.

Since the strength of the specimen varies during SRA due to the age hardening response, room temperature tensile tests were performed on the interrupted SRA tests to examine the strength variation, which is attributed to the precipitate evolution and thus can reflect the creep resistance variation.

Transmission electron microscopy (TEM) was conducted using Gatan691 on selected samples subjected to different SRA conditions: 7 h and 14 h SRA on 1% pre-strained samples with an initial stress of 320 MPa; 14 h SRA on a 3% pre-strained sample with an initial stress of 320 MPa; 14 h pure ageing (i.e. $\sigma_i$: 0MPa) on a 1% pre-strained sample. For TEM observation, 3 mm discs were punched from the selected samples and ground down to 60-70 um thickness after the room temperature tensile test. Subsequently these discs were ion thinned at 4 KeV with a gun angle of 8°, then at 3.5 KeV and 3.0 KeV with a gun angle of 3° and 2°, respectively, for final polishing.

## 3 Results

### 3.1 Stress relaxation behaviour with different initial stresses and different pre-strain levels

The influence of the initial stress level, $\sigma_i$, on the stress relaxation curves for 1 % pre-strained samples, is shown in Fig. 3 (a). The results are normalised by the initial stresses values and illustrated in Fig. 3 (b). In addition, these curves are re-plotted as percent stress reduction (%SR) vs. initial stress, $\sigma_i$, in Fig. 3 (c) to illustrate clearly the dependency of the percentage stress reduction (%SR) on the initial stress, for a range of

times $t$ = 6 hrs, 10hrs, 14hrs. Based on the unique 3-stage strain-stress-strain controlling route, the alloy exhibits a corresponding 3-stage stress relaxation behaviour.

Generally, the stress relaxation curves at Stage I exhibit a typical logarithmic stress relaxation behaviour, i.e. an initial rapid rate of relaxation to an approximately constant stress. This trend has also been observed extensively in literature, for example, Chen, et al. [17] reported the same logarithmic declined stress-time curve of an Al-Zn-Mg-Cu alloy in a simulated age forming test. Only a small stress reduction (%SR) of 1%-3% is observed in Stage I and no obvious variation in SR is seen for the different initial stresses. These limited SR values indicate that 120°C (i.e. $< 0.3T_{melt}$) is insufficient to exploit dislocation creep mechanisms. According to the deformation map from Ashby [24] and Somekawa et al. [25], diffusion creep is expected to dominate at a relatively lower temperature, and in addition, fine grain structure promote diffusion creep due to the increase in available vacancies and paths at grain boundaries. The phenomenon is also suggested in [26]. During SRA, the grain sizes of the SRA samples are initially small and, according to [16], are expected to simultaneously increase and elongate in the applied stress direction with the increase of the ageing time. Therefore, the creep mechanism at Stage I may be dominated by grain boundary diffusion, resulting in negligible %SR. Another possible reason for the limited stress reduction at Stage I is the simultaneous hardening phenomenon. The stress relaxation resistance at this stage is significantly increased due to the simultaneous thermally activated age-hardening as will be discussed in Section 3.2. Therefore, the alloy rapidly reaches its threshold stress as a result of the increased stress relaxation resistance.

Being stress controlled, the stresses remain constant in Stage II. In Stage III, the increased temperature (i.e. $170°C > 0.3T_{melt}$) releases the limitation of the creep deformation and being strain controlled, stress relaxation is occured again. A 13%-40% SR is observed with initial stress ranging from 220 MPa to 360 MPa at Stage III. Contrary to traditional relaxation curves, the stress relaxation behaviour at Stage III exhibits a unique characteristic which continuously decreases with no apparent threshold stress. In addition, dislocation creep mechanism dominates the stress relaxation behaviour at this stage due to the higher temperatures (i.e. $> 0.3T_{melt}$) and larger grain sizes according to the deformation map [24, 26]. Note that the creep mechanism in this stage will also be distinguished by the calculated the stress exponent $n$ (i.e. the slope of creep strain rate vs. stress in log-log scale). For dislocation creep, the stress relaxation resistance mainly depends on the precipitate size and distribution (as detailed in Section 3.3), which can be reflected by the yield strength variation (as detailed in Section 3.2). Therefore, the absence of the threshold stress at Stage III can be attributed to the simultaneous over-ageing phenomenon, which leads to a continuous decrease in the stress relaxation resistance. Fig. 3 (c) presents the total stress reduction in percent during SRA, which gives a direct %SR value under different initial stresses.

Fig. 4 (a) and (b) presents the experimental and the normalised the stress relaxation curves, respectively, under dynamic ageing conditions, comparing the influence of 0%, 1%, 3% pre-strain for an initial stress level of 320 MPa. Fig. 4(c) shows the pre-strain dependency of the stress reduction at a range of SRA times. Generally, the cold-stretching prior to SRA leads to a considerable enhancement in stress relaxation response,

which is in agreement with the results reported by Regensburger [22]. The total stress reduction increases from 25.9% to 38.8% was observed when the pre-strain level increases from 0% to 3%. According to Wimpory et al. [27] and Deschamps et al. [7, 28], a marked amount of dislocations can be generated inside the aluminium matrix by pre-strain. Therefore, the facilitated stress relaxation occurs as cold stretching generates more mobile dislocations which can increase the creep strain rate, directly obeying Orowan's equation. These pre-existing dislocations can also affect the creep strain rate indirectly by accelerating the precipitation evolution, leading to a faster increase in the stress relaxation resistance followed by an accelerated decrease post achieving the maximum value. The combined effects both from the dislocations and modified precipitation patterns result in the promotion of stress relaxation behaviour. However, comparing the stress relaxation behaviour at Stage I between the 0% and 1% pre-strained samples, greater stress reduction is generated by the un-pre-strained sample. Though the loading curves are not shown in Fig. 3, it has been observed that the SRA loading curves of the pre-strained samples are all linear, due to prior pre-strain hardening effects, but that plastic strain was generated on loading the SRA tests of the un-prestrained samples. This plastic loading strain leads to anelasticity [29] causing an enhancement on the stress relaxation behaviour at the very early in Stage I. However, the enhancement due to the anelasticity is smaller than that caused by 3% pre-strain treatment. Therefore, stress reduces more of a 3% pre-strained sample at Stage I. The slight fluctuation of the stress reduction with different pre-strained levels at 6h, illustrated in Fig. 4(c), should be attributed to anelasticity effect. While this effect becomes negligible at Stage III. Thus, larger SR is observed with higher pre-strain levels at 10 h and 14 h. A total stress reduction of 25.9% - 38.8% was observed after 14 h SRA under $\sigma_i$ = 320MPa with 0% - 3% pre-strain levels.

(a)

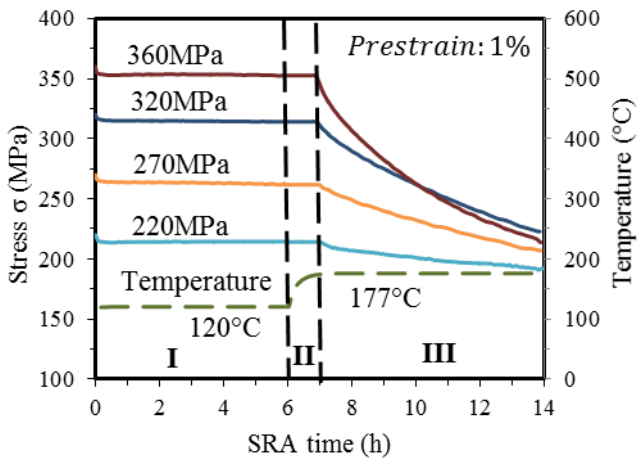

(b)

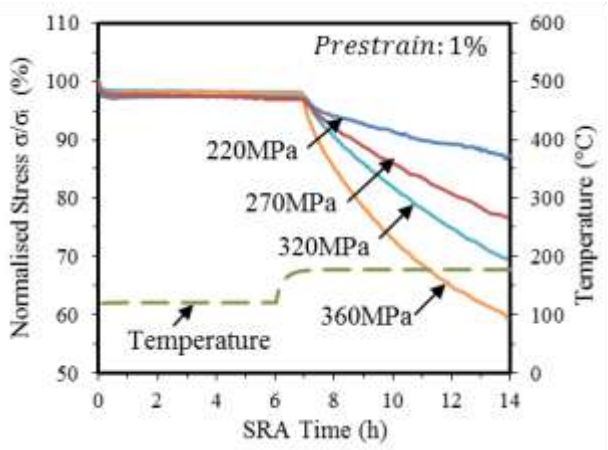


(c)

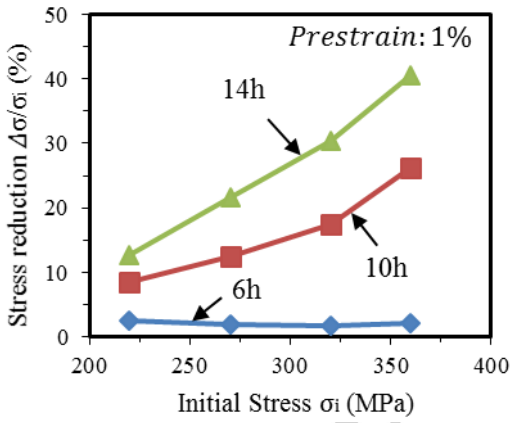


Fig. 3. (a)Stress relaxation curves ; (b) the curves shown in (a) normalised by the initial stresses under dynamic ageing conditions; the temperature variation is shown by the dashed line. (c) Initial stress dependency of the stress reduction (%SR) at time = 6 hrs, 10 hrs, 14 hrs.

(a)

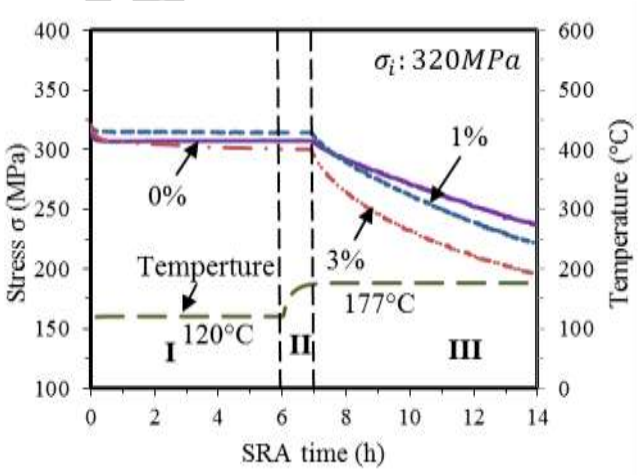

(b)

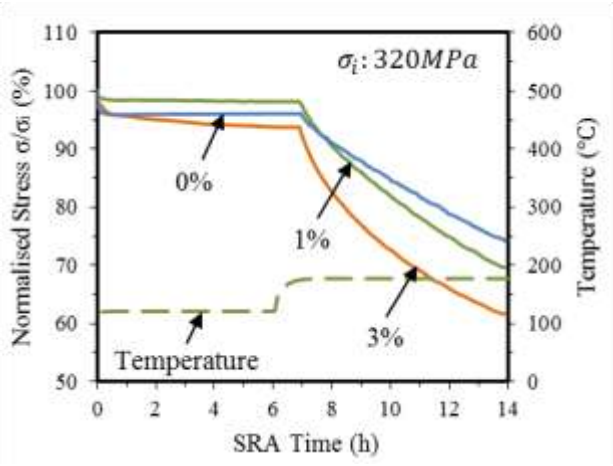


(c)

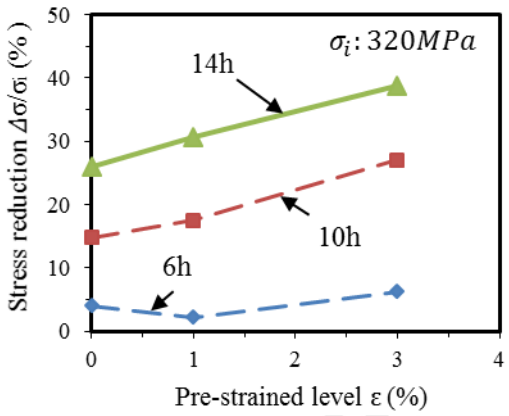


Fig. 4. (a) Stress relaxation curves; (b) the curves shown in (a) normalised by initial stresses under dynamic ageing conditions, the temperature variation is shown by the dashed line; (c) Pre-stretch dependency of the stress reduction (%SR) at t= 6hrs, 10hrs, 14hrs.

At Stage III, the sample's strain is held constant, and an estimate of the creep strain rate can be obtained. Neglecting any plasticity effects during SRA, it can be assumed that creep strain accumulation is accommodated for by a reduction in elastic strain, such that Eq. (3) is satisfied where $\varepsilon_T$, $\varepsilon_e$ and $\varepsilon_c$ are the total, elastic and creep strains, respectively. As generally accepted, stress relaxation can be regarded as a special form of creep behaviour. It is well established by a number of researchers, including Mostafa et al. [30-32], Tjong et al. [33], Chen et al. [17], Gupta et al. [34] etc., that the power-law creep equation, Eq.(4), may be used to describe dislocation creep behaviour. Therefore, equating Eq.(3) and Eq.(4), the creep strain rate vs stress relationship and the power-law stress exponent *n* (given by the slope of this plot ) during Stage III, which is of significant interest, has been deduced and is plotted (on a log-log axis) in Fig. 5. Information of the stress exponent *n* can be used to verify the creep mechanisms [26]. In this case *n* appears unchanged with initial stress levels. However, *n* values are found to marginally increase with increasing pre-strained levels, ranging from 3.1 to 3.5, though some variability in the data is expected. These values of *n* indicate that dislocation creep dominates the SRA process at Stage III [26, 30]. In addition, the increasing *n* value illustrated in Fig. 5(b) suggests that the initial dislocations induced by pre-strain treatments can vary the dislocation creep mechanisms slightly, from solute-drag dominated creep to climb-controlled dominated [26].

$$\varepsilon_T = \varepsilon_c + \varepsilon_e = constant \tag{1}$$

$$=> \frac{d\varepsilon_T}{dt} = 0 = \dot{\varepsilon}_c + \dot{\varepsilon}_e \tag{2}$$

$$\dot{\varepsilon}_e = -\dot{\varepsilon}_c = -\frac{d\sigma}{E \cdot dt} \tag{3}$$

$$\dot{\varepsilon}_c = A\sigma^n exp\left(-\frac{Q}{RT}\right) \tag{4}$$

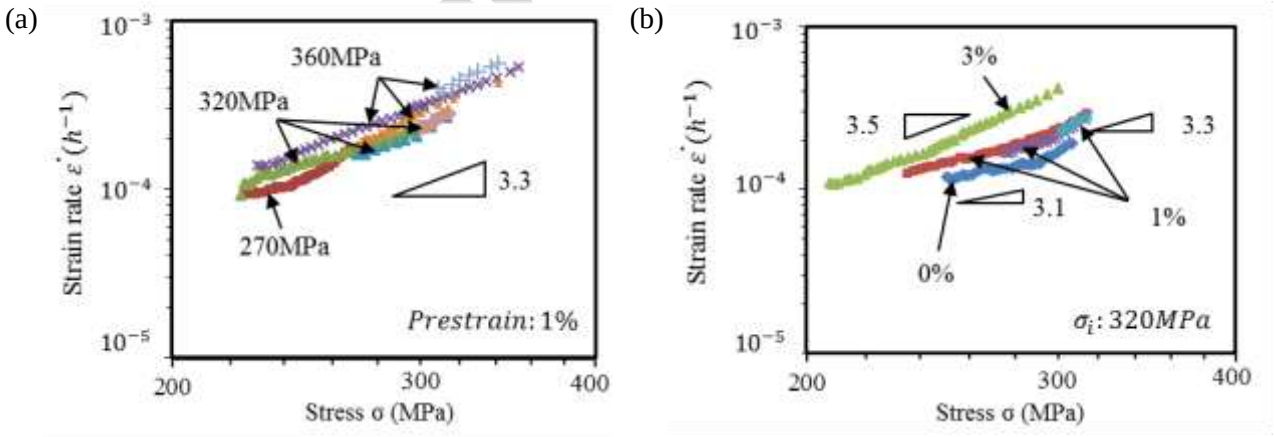


Fig. 5. Creep strain rate-stress curves at Stage III under (a) 1% pre-strain at various initial stresses, (b) 0%, 1%, 3% pre-strains at an initial stress of 320 MPa.

### 3.2 Age hardening behaviour with different initial stresses and different pre-strain levels

Fig. 6 (a) illustrates the yield strength evolution, which is attributed to the dynamic precipitation process during SRA, of 1% pre-strained material for different initial stresses. It is generally accepted that a period of time at low temperature (Stage I) benefits the nucleation of finely distributed GP zones, while a subsequent high-temperature stage leads to a fast growth on the pre-existing precipitates [6, 11, 35]. The yield strength evolution reflects the multi-step ageing kinetics, which gradually increases at Stage I, rapidly reaches its peak (i.e. T6 temper) after the up-quenching Stage II, and decreases subsequently to a T74 over-aged temper. Moreover, it can be shown that the yield strength variation is generally uninfluenced by the different initial stresses at Stage I, due to negligible creep strain generation, which has been discussed in Section 3.1. Note that the pure-aging curve refers to a test where no load was applied to the sample during SRA. However, at Stages II & III, where a notable increase of creep strain is present, the ageing response is enhanced, and a peak strength is attained at a shorter time in the SRA samples compared to the pure-aging sample. This enhanced strength in the SRA tests is short-lived and it rapidly decreases below that of the pure ageing sample at the time of ~8 hrs. It has been widely reported [7, 13] that dislocations can alters the precipitate evolution, leading to a faster precipitate nucleation and growth on both dislocations and grain boundaries. Therefore, the increasing dislocations, introduced by increasing creep strains simultaneously, lead to a dynamic effect on promoting the ageing response. Fig. 6(b) provides a clear illustration of the relationship between initial stresses and the final T74 yield strength at 14 hrs, which is of significant interest. Resulting from the considerable ageing promotion, the yield strength under higher initial stresses exhibit lower values after SRA. A 45 MPa decrease in the yield strength, compared to the case of pure aging, is obtained when the initial stress is 360 MPa.

The pre-strain effect on the ageing kinetics has been studied by comparing its influence on the yield strength variation between un-pre-strained and 1% pre-strained samples during pure ageing as shown in Fig. 7. Pre-strains mainly affects the precipitation process by accumulating more dislocations ahead of SRA, thus resulting in a noticeable accelerated age hardening response at the beginning of SRA. It can be seen that the yield strength of 1% pre-strained sample is initially 60 MPa higher than the non-pre-strained sample. This phenomenon occurs due to two reasons. The first is the strain hardening effects, due to dislocations entanglements, which caused a 25 MPa strength increase. For clarity, the 25 MPa strength increase was obtained by comparing the room temperature yield strengths of the post quenching sample and the post quenching + 1% pre-strain sample. The second reason is the promoted age hardening effects During the heating–up period from room to 120 °C (which for clarity is not shown in the figure) the dislocations in the 1% pre-strained sample act as favourable nucleation sites, thus accelerating the age strengthening effects resulting in a 35 MPa increase in the 1% pre-strained sample's yield strength. This promotion effects decreased gradually and finally more or less disappeared at the end of Stage I. At Stage II and III, no obvious yield strength variation is observed.

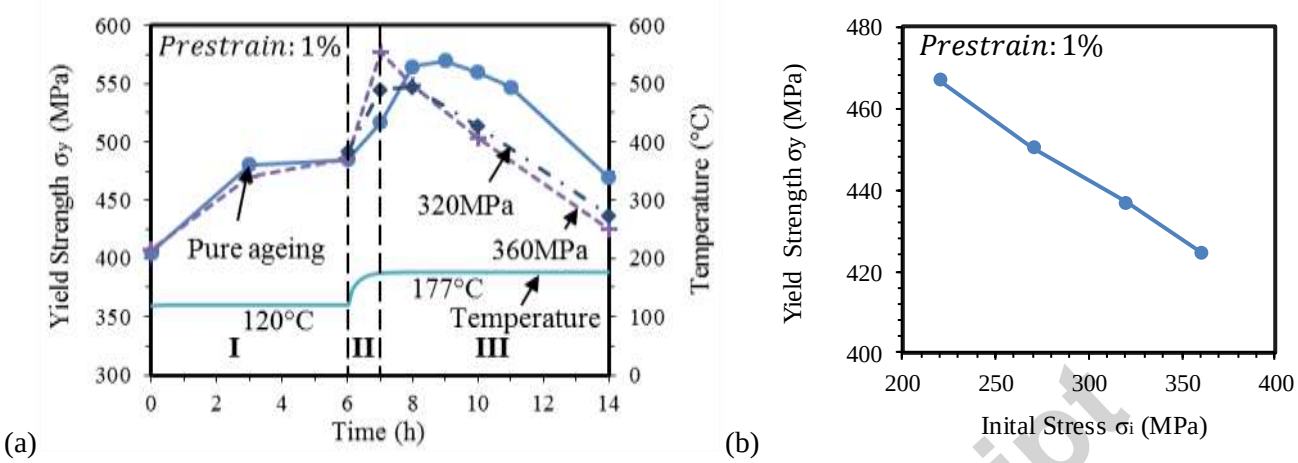


Fig. 6. Yield strength curves under dynamic ageing conditions: (a) yield strength vs. SRA time (b) initial stress dependency of the yield strength at 14 hrs. The results were obtained through room temperature tensile tests on interrupted SRA samples. All samples were pre-stretched to 1%.

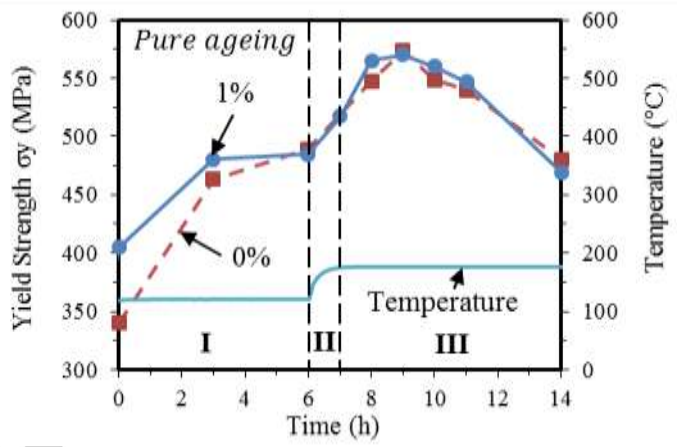


Fig. 7. Yield strength vs. SRA time during pure ageing. The test specimens are initially pre-stretched to 0% and 1% at room temperature, then are subjected to the sequential ageing treatment at 120 °C for 6h followed by 177 °C for 7h.

### 3.3 TEM characterization on selected stress relaxation aged samples

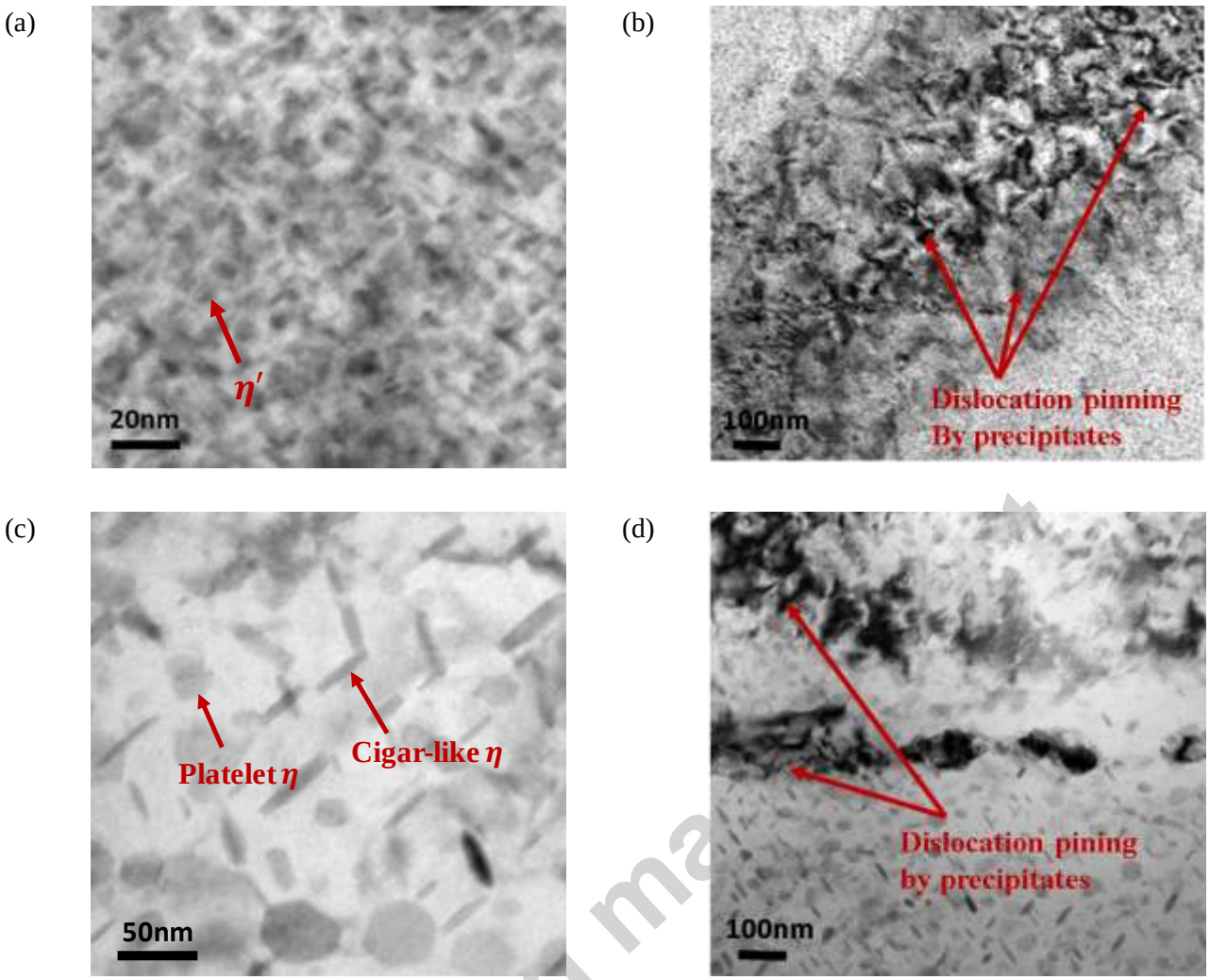


Fig. 8 Bright field TEM images of samples after (a), (b) 7 h and (c), (d) 14h stress relaxation ageing treatment with an initial stress of 320 MPa. Both samples were initially pre-strained to a total strain of 1%

Fig. 8 presents the TEM images of 1% pre-strained samples under 2 conditions: (a) and (b) 7 h stress relaxation ageing (i.e. peak-aged); (c) and (d) 14 h stress relaxation ageing (i.e. T74 over-aged). The initial stress for both conditions is 320 MPa. Finely dispersed $\eta'$ are observed for samples after 7 h SRA in Fig. 8 (a). These small precipitates (i.e. GP zones and $\eta'$) are around 10 nm in size, which is equal to the average critical size of the aluminium alloy. Precipitates with an average critical size can provide the highest cutting resistance to the dislocation motion while avoid the dislocation bowing [36]. In addition, an extremely large precipitate density is observed, which leads to more precipitates hindering the dislocation movement. Therefore, dislocations are firmly pinned when entangled with the large amount of small precipitates, resulting in the largest yield strength and stress relaxation resistance of the sample. Cigar-like and platelet morphology $\eta$ are observed after 14 h SRA in Fig. 8 (c). Compared to the precipitates in Fig. 8 (a), the precipitates are larger in

size, ranging from around 20 nm to 30 nm, while smaller in density. When the size of the precipitates are larger than its critical size (i.e. ~ 10 nm [36]), Orowan strengthening mechanism dominates, where the material strength is inversely proportional to the precipitate size. Dislocations can easily by-pass the precipitates using less energy. Therefore, the larger precipitates with a smaller density lead to a reduction in sample's strength and stress relaxation resistance. The coarsening precipitate evolution from 7 h, Fig. 8 (a), to 14 h, Fig. 8 (c), in SRA are in accordance with the decreasing yield strength evolution shown in Fig. 6. Fig. 8 (b) and (d) present the precipitate distributions around the dislocations. It can be observed that large amount of precipitates gather on and around dislocations. These precipitates are a mix of $\eta'$ and $\eta$ with relatively large sizes. Two key facts are demonstrated here: precipitates are favoured to nucleate and grow in and around dislocations (i.e. line defects containing voids as nucleation favourite sites); precipitates can pin the dislocations and resist the deformation. These two findings support the results in Section 3.1 and 3.2 that 'dislocation creep' mechanism dominated the stress relaxation process in Stage III and dislocations promoted the ageing response during SRA.

(a)

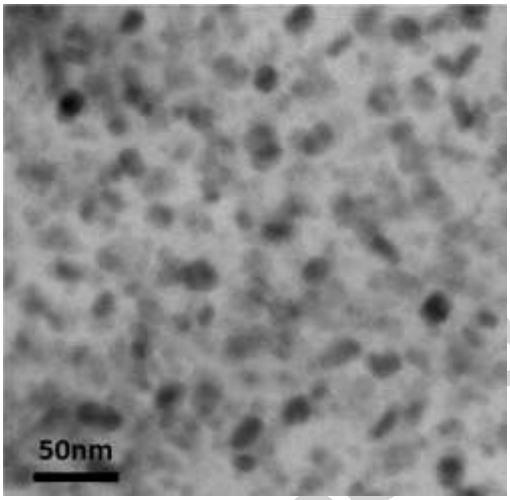


(b)

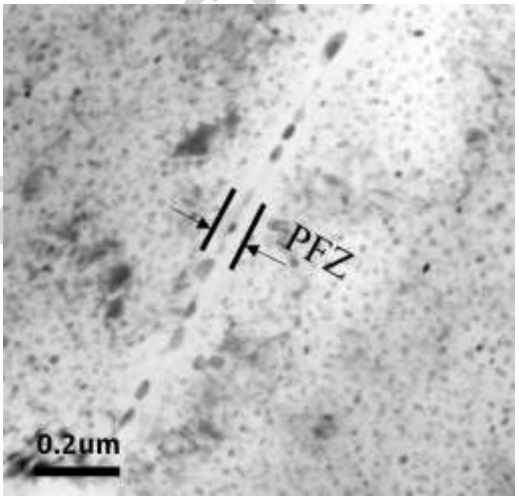


(c)

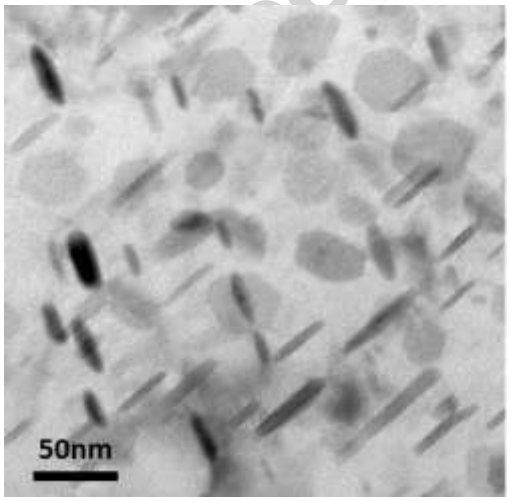


(d)

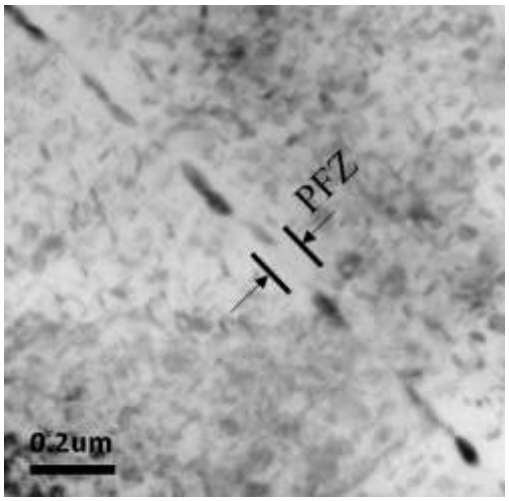

(e) (f)

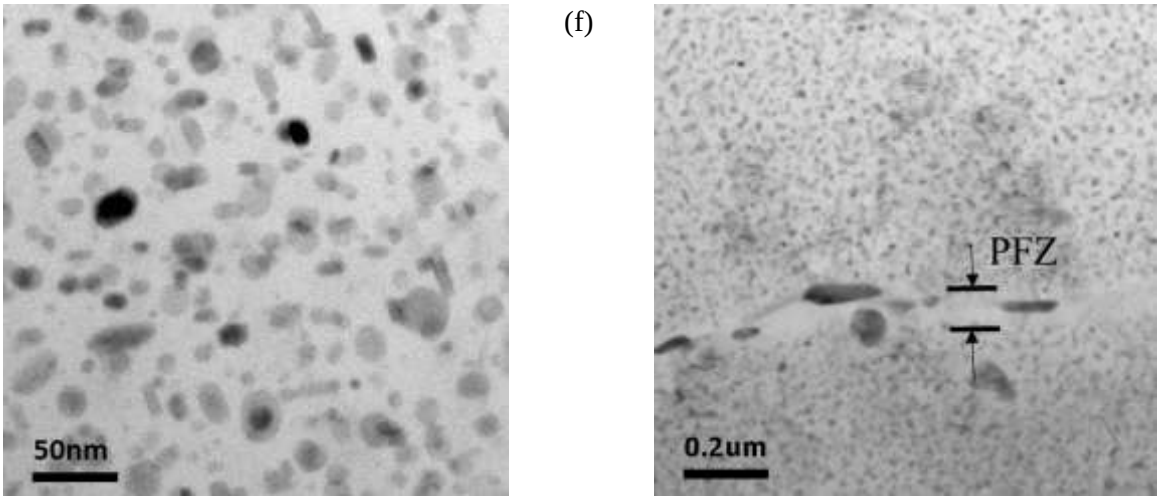


Fig. 9 Bright field TEM images of samples after 14h stress relaxation ageing treatment: (a), (b) 1% - 0MPa; (c), (d) 1% - 320MPa; (e), (f) 3% - 320MPa. Note that e.g. 1%-320MPa indicates the sample was initially pre-strained to 1% and the initial stress $\sigma_i$ for SRA is 320MPa. The precipitate free zones (PFZ) were labelled.

Three samples (i.e. 1%-0 MPa, 1%-320 MPa, 3%-320 MPa) after 14 h stress relaxation ageing (i.e. T74) were selected out for examining the precipitate distributions using TEM. The bright field TEM results are shown in Fig. 9. Note that e.g. 1%-320 MPa indicates the sample was pre-strained to 1% before SRA and the initial stress,$(\sigma_i)$ for SRA is 320MPa. Fig. 9 (a) and (b) illustrate the precipitate patterns in the aluminium bulk matrix and along grain boundaries respectively for the 1%-0 MPa sample after the T74 treatment. In the bulk matrix, the precipitates are 15-20 nm in size and the majority of them are in platelet morphology, while the precipitates on grain boundaries are 2-3 times larger and around 40-60 nm in size. The width of grain boundary precipitate free zones (PFZs), labelled in Fig. 9(b), are around 75 nm. Fig. 9(c) and (d) provide the TEM images on the 1%-320 MPa sample after the T74 treatment. The bulk precipitates are around 20-30 nm, while grain boundary precipitates are extremely large with sizes ranging from 80-170 nm. The PFZs are around 100nm. Comparing Fig. 9 (a, c) and (b, d), one can observe that the T74 1%-320 MPa sample contains larger precipitates with smaller density than the T74 1%-0 MPa sample. The observation provides evidence that the higher initial stress facilitates the precipitate evolution, resulting in coarser precipitates after T74 SRA and thus lower yield strength (in accordance with the yield strength comparison shown in Fig. 6(b)). Fig. 9(e) and (f) show the precipitate distributions of the 3%-320 MPa sample after T74 treatment. The precipitate density and PFZs are nearly the same with that of the 1%-320 MPa sample. This finding agrees with the results in Fig. 7 that pre-dislocation effects gradually disappear with ageing time. However, most bulk precipitates of the 3%-320 MPa sample have platelet morphology in contrary to that of the 1%-320 MPa sample which have cigar-like morphology. The grain boundary precipitates are larger than that shown in Fig. 9(d).

## 4 Discussion

In contrast to traditional relaxation curves, as reported by Chen [17] and Pommier [37] where 2–3 different *n* values can be deduced from the relaxation data using the traditional power-law creep function owing to the threshold stress, only one *n* value was obtained at Stage III. The absence of a threshold stress at Stage III is primarily attributed to the over-aged precipitate evolution, which is activated by the high temperature. The continuous over-aged evolution of precipitates, described in Section 3.2 and validated using TEM images in Section 3.3, provides less dislocation pining effects and therefore leads to a gradual decrease in stress relaxation resistance with time. Simultaneously, the creep strain accumulation affects the precipitation process by introducing defects including dislocations and vacancies. These coupling effects between precipitation and stress relaxation are schematically illustrated in Fig. 10. The general trend of the strength during SRA, which is capable of quantifying the effects of precipitations on the stress relaxation resistance, is similar to the results of several papers [8, 11, 38-40] studying the static ageing evolution. Therefore, although only the peak aged and T74 over aged samples were selected for observing the precipitate distributions (i.e. Fig. 8 and Fig. 9), the precipitate evolution should be similar to that in the literature. The evolution of precipitates and material strength corresponding to the SRA treatment can be divided into 3 regions — (i) a nucleation region ($t_1$ - $t_3$) where evenly-distributed small GP (I) & (II) zones, generated from super-saturated-solid-solution (SSSS), benefit the yield strength by pinning dislocation movements; (ii) a growth region ($t_3$-$t_4$) where ordered $\eta'$ forms rapidly on the pre-existing GP zones, the yield strength increases to its peak value; (iii) a coarsening region ($t_4$ - $t_5$) where precipitates continuously increase in size and decrease in density, providing a decreasing resistance to dislocation motion and hence yield strength. In terms of the stress relaxation process, which as previously described is classified by strain-stress-strain control, Stage I completely coincides with the nucleation region. Thus the stress rapidly reaches its threshold value as precipitate nucleation occurs, leading to an increasing resistance to the creep strain generation. In contrast, Stage III contains only a small part of the growth region and the whole coarsening region, which implies an initial slight increase in the stress relaxation resistance is followed by a rapid decrease. Thus, the decreased resistance leads to continuous stress relaxation behaviour. According to the reports from Somekawa [26], dislocation creep varies from solute drag creep to climb-controlled creep when *n* increases from 3 to 5. Hence, dislocation creep mechanism is expected to dominate at Stage III, as indicated by the *n* value ~3.3 obtained in Fig. 5.

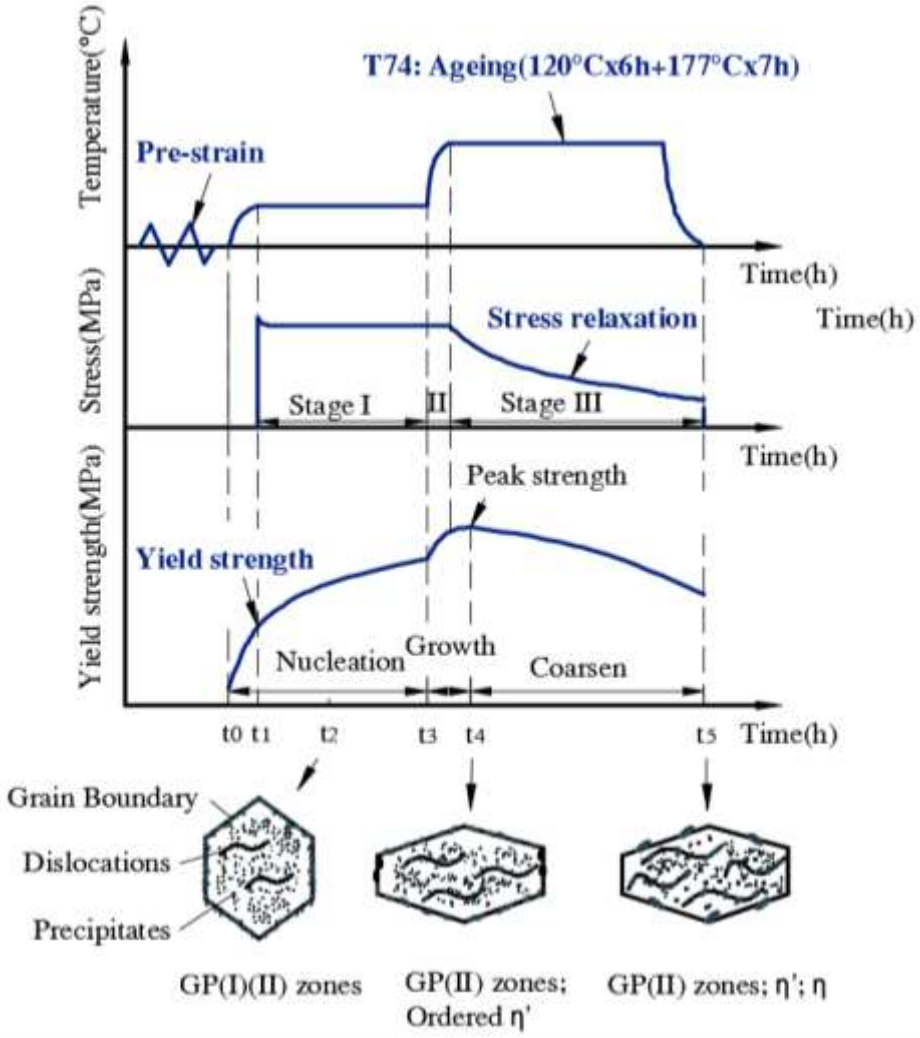


Fig. 10. Schematic diagram illustrating the stress relaxation, yield strength and precipitation evolution under T74 multi-step dynamic ageing conditions

### 4.1 Initial stress effects on SRA behaviour

It has been reported that higher stresses during creep-ageing can not only facilitate the formation of precipitates but also accelerate the creep strain generation [1]. However, from the relaxation-ageing phenomena shown in Fig. 3(a) and Fig. 6(a), the initial stress has little effect on both the stress relaxation and ageing behaviour observed at Stage I, while significant influence was observed at Stage III. This indicates that the temperature ($< 0.3T_{melt}$) in Stage I is below that required for significant creep to occur. Ageing is also hardly affected by the initial stresses during Stage I due to the negligible creep strain-induced dislocations. Although larger initial stresses in the elastic region do create larger lattice spaces, which benefits the diffusion of the atoms, the effects on the precipitate evolution observed are negligible. However, when the temperature is increased and dislocation creep mechanism dominates the process in Stage III, the effects of initial stresses becomes considerable. Larger stress reductions were obtained under higher initial stresses. Larger amount of

dislocations were created by creep with higher initial stresses, resulting in an acceleration in the precipitate evolution, and thus a lower stress relaxation resistance & yield strength after $t = \sim 8h$ (Fig. 6). Hence stress relaxation is assisted by the precipitate patterns and reduced dislocation pinning effects. The accelerated precipitate evolution is validated in Fig. 9(a-d) through conducting TEM tests on the samples after T74 SRA treatment with $\sigma_i$ =0MPa and 320MPa. Both the bulk and the grain boundary precipitates of the 1%-320MPa sample are larger than that of the 1%-0 MPa sample. The re-distributed precipitate pattern (i.e. larger precipitate sizes, smaller precipitate density), which results from creep induced dislocations and dictates the mechanical properties, leads to an easier dislocation movement when encountered with fewer bulk precipitates and thus a faster stress relaxation. The value of *n* is unaffected by different initial stresses examined during SRA, indicating that these initial stresses do not alter the relaxation mechanisms.

### 4.2 Pre-strain effects on SRA behaviour

The pre-strain effects on the subsequent ageing response have been widely studied [7, 13]. It is commonly agreed that the material is noticeably strengthened by dislocation hardening and the ageing response is dramatically accelerated at the early stage. Similar influences were found in this study shown in Fig. 7. In terms of the effects on relaxation process illustrated in Fig. 4, the cold work prior to SRA lead to a larger %SR. Based on the brief discussion in Section 3.1, one can conclude that the positive or negative effects of pre-strain levels on SR behaviour depend on the complicated precipitate-dislocation interactions and also dislocation-dislocation interactions. In this case, the positive effects dominate, which indicates that the dislocations were created evenly and flow uniformly during the process. Thus, in Stage I, although the stress relaxation resistance of the samples with higher pre-strained values is larger than that with lower pre-strained values at a same selected time, represented by the yield strength shown in Fig. 7, the negative effects from the increasing resistance to the stress relaxation and dislocation tangle cannot keep pace with positive effects from the increase in the quantity of the dislocations.

In Stage III, the effects of pre-strain levels on the material strength response were experimentally examined through employing room temperature tensile tests on pure aged samples (Fig. 7) and employing TEM on stress relaxation aged ($\sigma_i$=320MPa) samples (Fig. 9 c-f) post different pre-stretch levels. For pure aged samples, no pre-strain effects were seen in Stage III where the yield strength evolution was almost the same post 0% and 1% pre-strain levels (i.e. Fig. 7). In terms of stress relaxation aged samples ($\sigma_i$=320MPa), results (Fig. 9 c-f) show that larger grain boundary precipitates were formed in the sample with higher pre-strain levels after T74 SRA, while slight similar bulk precipitate patterns (i.e. density, PFZs, etc.) were observed. In addition, the morphology of the precipitates formed under 1%-320 MPa and 3%-320 MPa are slightly different. However, the yield strength (i.e. 414 MPa) of the 3%-320 MPa sample is slightly lower than that (i.e. 437MPa) of the 1%-320 MPa (For clarify, not shown in the results). The TEM observation and the yield strength results suggest that pre-strain, somewhat, can slightly affect the precipitate distribution and reduce the precipitation hardening response after T74 ageing treatment. However, the influence is not significant

especially for pure aged samples. Based on the results and discussion on pure ageing and SRA ($\sigma_i$=320MPa) with different pre-strained values, one can conclude that the facilitated stress relaxation caused by high pre-strain levels at Stage III is primarily attributed to the increase in the dislocation density.

The stress relaxation data during Stage III has been further examined as shown in Fig. 11. The stress relaxation rates are plotted in solid lines and stress relaxation curves are plotted in dotted lines. It can be seen that different pre-stretch levels affect the initial stress relaxation rate, however, after 11 hrs the stress relaxation rate becomes constant ($\neq 0$) and independent of both pre-strain value and the remaining stresses. This suggests that the dramatic reduction in the yield strength and precipitate coarsening controls the stress reduction rate at times greater than 11 hours, as opposed to creep.

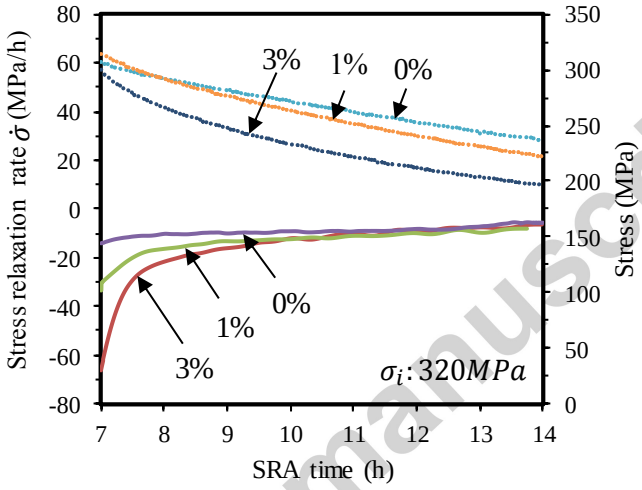


Fig. 11. Stress relaxation (dotted lines) and its rate (solid lines) curves at stage III under dynamic ageing conditions. The test specimens are initially pre-stretched to 0%, 1%, and 3% at room temperature, and are subjected to the sequential stress relaxation ageing (SRA) treatment at 120 $^{o}$C for 6 h followed by 177 $^{o}$C for 7 h. The initial stress is 320 MPa.

## 5 Conclusions

The stress relaxation ageing (SRA) behaviour of AA7050 has been experimentally examined and microstructurally validated under multi-step dynamic ageing conditions with different initial stresses ($\sigma_i$) post different pre-strained levels. Two different stress relaxation characteristics have been observed at 120°C and 177 °C, respectively. The following conclusions can be made:

1. As expected, the temperature is the primary influencing factor for SRA behaviour. Higher temperature results in a larger stress reduction (SR). It has been found that 120 °C is too low for significant stress relaxation. SRA at 120°C generates a negligible amount of creep strains in Stage I, which is about 6-20 times smaller than that at 177°C (i.e. SR: 10-38.5%) in Stage III.

2. Initial stress ($\sigma_i$) has a negligible effect on stress relaxation behaviour at 120°C but dramatically accelerates the stress relaxation behaviour at 177°C. An increase in the SR from 13% to 40% has been observed when $\sigma_i$ increased from 220MPa to 360MPa.

3. The stress relaxation behaviour is enhanced by larger pre-strain levels. A 38.8% total stress reduction after SRA with $\sigma_i$=320MPa was observed using a 3% pre-strained sample, which is 1.5 times larger than that using an un-strained sample. The enhancement is mainly caused by the positive effects from plastic strains induced dislocations. The stress relaxation rate was significantly increased by higher pre-strain levels in the early part of Stage III, while it plateaued to a constant value, in-dependent of the pre-strain levels, after 11hrs.

4. The stress exponent *n* has been found generally unaffected by the different initial stresses ($\sigma_i$) in Stage III. However, *n* varies from 3.1-3.5 with increased pre-strained levels. The *n* values suggest a 'dislocation creep' mechanism.

5. The age hardening evolution is promoted by both the pre-stretch treatment and the stress relaxation process. It has been found that the pre-stretch treatment mainly affects the precipitation process at the beginning of Stage I by creating more nucleation sites. While the stresses during SRA start to impact the precipitation evolution from Stage II. Higher initial stresses($\sigma_i$) introduce larger creep strains, thus leading to a faster growth and coarsening of the precipitates. The precipitate size after T74 SRA ($\sigma_i$=320MPa) has been observed around 1.5 times larger (i.e. 20-30nm) than that (i.e. 15-20nm) after T74 pure ageing ($\sigma_i$=0MPa). The yield strength after T74 SRA ($\sigma_i$=220-360MPa) has been found up to 10% lower than that after T74 pure ageing.

**Acknowledgements**

The strong support from The Aviation Industry Corporation of China (AVIC) the First Aircraft Institute (FAI) and International Science & Technology Cooperation Program of China (Grant Nos. 2014DFA51250) for this funded research is much appreciated. The research was performed at the AVIC Centre for Structural Design and Manufacture at Imperial College London.

## Reference

[1] L.H. Zhan, J.G. Lin, T.A. Dean, M.H. Huang, Experimental studies and constitutive modelling of the hardening of aluminium alloy 7055 under creep age forming conditions, International Journal of Mechanical Sciences 53(8) (2011) 595-605.
[2] L. Ph, L. Ph, W. T, Aluminium alloy development for the airbus A380 – part 1. , Advanced Materials & Processes 165(6) (2007) 3.
[3] R. Pan, Z. Shi, C.M. Davies, C. Li, M. Kaye, J. Lin, An integrated model to predict residual stress reduction by multiple cold forging operations in extra-large AA7050 T-section panels, Journal of Engineering Manufacture (2016)
[4] J.S. Robinson, D.A. Tanner, C.E. Truman, R.C. Wimpory, Measurement and Prediction of Machining Induced Redistribution of Residual Stress in the Aluminium Alloy 7449, Experimental Mechanics 51(6) (2011) 981-993.
[5] S. Esmaeili, D.J. Lloyd, W.J. Poole, A yield strength model for the Al-Mg-Si-Cu alloy AA6111, Acta Materialia 51(8) (2003) 2243-2257.
[6] W.J.S. Poole, H R; Castillo, T., Process model for two step age hardening of 7475 aluminium alloy, Materials Science and Technology 13 (1997) 897-904.
[7] A. Deschamps, F. Livet, Y. Bréchet, Influence of predeformation on ageing in an Al–Zn–Mg alloy—I. Microstructure evolution and mechanical properties, Acta Materialia 47(1) (1998) 281-292.
[8] O.R. Myhr, Ø. Grong, Modelling of non-isothermal transformations in alloys containing a particle distribution, Acta Materialia 48(7) (2000) 1605-1615.
[9] G. Sha, A. Cerezo, Early-stage precipitation in Al–Zn–Mg–Cu alloy (7050), Acta Materialia 52(15) (2004) 4503-4516.
[10] D. Dumont, A. Deschamps, Y. Brechet, On the relationship between microstructure, strength and toughness in AA7050 aluminum alloy, Materials Science and Engineering: A 356(1–2) (2003) 326-336.
[11] K. Stiller, P.J. Warren, V. Hansen, J. Angenete, J. Gjønnes, Investigation of precipitation in an Al–Zn–Mg alloy after two-step ageing treatment at 100° and 150°C, Materials Science and Engineering: A 270(1) (1999) 55-63.
[12] W. Guo, J. Guo, J. Wang, M. Yang, H. Li, X. Wen, J. Zhang, Evolution of precipitate microstructure during stress aging of an Al–Zn–Mg–Cu alloy, Materials Science and Engineering: A 634 (2015) 167-175.
[13] G. Waterloo, V. Hansen, J. Gjønnes, S.R. Skjervold, Effect of predeformation and preaging at room temperature in Al–Zn–Mg–(Cu,Zr) alloys, Materials Science and Engineering: A 303(1–2) (2001) 226-233.
[14] N. Han, X. Zhang, S. Liu, B. Ke, X. Xin, Effects of pre-stretching and ageing on the strength and fracture toughness of aluminum alloy 7050, Materials Science and Engineering: A 528(10–11) (2011) 3714-3721.
[15] W. Guo, M. Yang, Y. Zheng, X. Zhang, H. Li, X. Wen, J. Zhang, Influence of elastic tensile stress on aging process in an Al–Zn–Mg–Cu alloy, Materials Letters 106 (2013) 14-17.
[16] J.F. Chen, L. Zhen, J.T. Jiang, L. Yang, W.Z. Shao, B.Y. Zhang, Microstructures and mechanical properties of age-formed 7050 aluminum alloy, Materials Science and Engineering: A 539 (2012) 115-123.
[17] J.F. Chen, J.T. Jiang, L. Zhen, W.Z. Shao, Stress relaxation behavior of an Al–Zn–Mg–Cu alloy in simulated age-forming process, Journal of Materials Processing Technology 214(4) (2014) 775-783.

[18] J.K. Solberg, H. Thon, Stress relaxation and creep of some aluminium alloys, Materials Science and Engineering 75(1) (1985) 105-116.
[19] T.W. Spence, M.M. Makhlouf, The effect of machining-induced residual stresses on the creep characteristics of aluminum alloys, Materials Science and Engineering: A 630 (2015) 125-130.
[20] Y.Q. Wang, M.W. Spindler, C.E. Truman, D.J. Smith, Critical analysis of the prediction of stress relaxation from forward creep of Type 316H austenitic stainless steel, Materials & Design 95 (2016) 656-668.
[21] D.F. Li, N.P. O'Dowd, C.M. Davies, K.M. Nikbin, A review of the effect of prior inelastic deformation on high temperature mechanical response of engineering alloys, International Journal of Pressure Vessels and Piping 87(10) (2010) 531-542.
[22] J. Regensburger, N. Cwiekala, C. Albiez, W.-G. Drossel, Pre-strain dependent relaxation behaviour of AA6016 during automotive paint drying processes, Production Engineering 10(2) (2016) 113-118.
[23] N.K. Sinha, S. Sinha, Stress relaxation at high temperatures and the role of delayed elasticity, Materials Science and Engineering: A 393(1–2) (2005) 179-190.
[24] M.F. Ashby, A first report on deformation-mechanism maps, Acta Metallurgica 20(7) (1972) 887-897.
[25] D.C. Stouffer, L. Thomas Dame, Inelastic deformation of metals : models, mechanical properties, and metallurgy, Wiley, New York, Chichester, Brisbane, Toronto, Singapore, 1996.
[26] H. Somekawa, K. Hirai, H. Watanabe, Y. Takigawa, K. Higashi, Dislocation creep behavior in Mg–Al–Zn alloys, Materials Science and Engineering: A 407(1–2) (2005) 53-61.
[27] R. Wimpory, F. Biglari, R. Schneider, K. Nikbin, N. O'Dowd, Effect of Residual Stress on High Temperature Deformation in a Weld Stainless Steel Materials Science Forum 524-525 (2006) 311-316.
[28] A. Deschamps, Y. Brechet, Influence of predeformation and agEing of an Al–Zn–Mg alloy—II. Modeling of precipitation kinetics and yield stress, Acta Materialia 47(1) (1998) 293-305.
[29] A. Rao, P. John Bouchard, S.M. Northover, M.E. Fitzpatrick, Anelasticity in austenitic stainless steel, Acta Materialia 60(19) (2012) 6851-6861.
[30] M.M. Mostafa, G.S. Al-Ganainy, A.M.A. El-Khalek, R.H. Nada, Steady-state creep and creep recovery during transformation in Al–Zn alloys, Physica B: Condensed Matter 336(3–4) (2003) 402-409.
[31] A.M. Abd El-Khalek, Steady state creep and creep recovery behaviours of pre-aging Al–Si alloys, Materials Science and Engineering: A 500(1–2) (2009) 176-181.
[32] M.M. Mostafa, M.M. El-Sayed, H.A. El-Sayed, H. Abd-Elaleem, Steady state creep during transformation in Al–1 wt.%Cu alloy, Materials Science and Engineering: A 518(1–2) (2009) 97-99.
[33] S.C. Tjong, Z.Y. Ma, Creep behaviour of precipitation-hardened ferritic Fe–19Cr–4Ni–2Al alloy, Materials Letters 56(1–2) (2002) 59-64.
[34] V.K. Gupta, S.B. Singh, H.N. Chandrawat, S. Ray, Steady state creep and material parameters in a rotating disc of Al–SiCP composite, European Journal of Mechanics - A/Solids 23(2) (2004) 335-344.
[35] Z. Li, B. Xiong, Y. Zhang, B. Zhu, F. Wang, H. Liu, Investigation of microstructural evolution and mechanical properties during two-step ageing treatment at 115 and 160 °C in an Al–Zn–Mg–Cu alloy pre-stretched thick plate, Materials Characterization 59(3) (2008) 278-282.
[36] I.J. Polmear, 3 - Wrought aluminium alloys, in: I.J. Polmear (Ed.), Light Alloys (Fourth Edition), Butterworth-Heinemann, Oxford, 2005, pp. 97-204.
[37] H. Pommier, E.P. Busso, T.F. Morgeneyer, A. Pineau, Intergranular damage during stress relaxation in AISI 316L-type austenitic stainless steels: Effect of carbon, nitrogen and phosphorus contents, Acta Materialia 103 (2016) 893-908.
[38] R. Arabi Jeshvaghani, H. Zohdi, H.R. Shahverdi, M. Bozorg, S.M.M. Hadavi, Influence of multi-step heat treatments in creep age forming of 7075 aluminum alloy: Optimization for springback, strength and exfoliation corrosion, Materials Characterization 73 (2012) 8-15.
[39] O.R. Myhr, Ø. Grong, H.G. Fjær, C.D. Marioara, Modelling of the microstructure and strength evolution in Al–Mg–Si alloys during multistage thermal processing, Acta Materialia 52(17) (2004) 4997-5008.
[40] Y.C. Lin, J.-L. Zhang, M.-S. Chen, Evolution of precipitates during two-stage stress-aging of an Al-Zn-Mg-Cu alloy, Journal of Alloys and Compounds 684 (2016) 177-187.